

Numerical simulation of heat transfer in a micro channel heat sinks using nanofluids

E. Farsad · S. P. Abbasi · M. S. Zabihi ·
J. Sabbaghzadeh

Received: 17 July 2010 / Accepted: 20 November 2010 / Published online: 8 December 2010
© Springer-Verlag 2010

Abstract In this study, a numerical simulation of copper microchannel heatsink (MCHS) using nanofluids as coolants is presented. The nanofluid is a mixture of pure water and nanoscale metallic or nonmetallic particles with various volume fractions. Also, the effects of various volume fractions, volumetric flow rate and various materials of nanoparticles on the performance of MCHS have been developed. A three-dimensional computational fluid dynamics model was developed using the commercial software package FLUENT, to investigate the conjugate fluid flow and heat transfer phenomena in micro channel heatsinks. The results show that the cooling performance of a microchannel heat sink with water based nanofluid containing Al_2O_3 (vol 8%) is enhanced by about 4.5% compared with micro channel heatsink with pure water. Nanofluids reduce both the thermal resistance and the temperature difference between the top (heated) surface of the MCHS and inlet nanofluid compared with that pure water. The cooling performance of a micro channel heat sink with metal nanofluids improves compared with that of a micro channel heat sink with oxide metal nanofluids because the thermal conductivity of metal nanofluid is higher than oxide metal nanofluids. Micro channel heat sinks with nanofluids are expected to be good candidates as the next generation cooling devices for removing ultra high heat flux.

List of symbols

c_p	Specific heat at constant pressure ($\text{J kg}^{-1} \text{K}^{-1}$)
h	Surface heat transfer coefficient (SHTC) ($\text{W m}^{-2} \text{K}^{-1}$)
K, k	Heat conduction coefficient ($\text{W m}^{-1} \text{K}^{-1}$)
Kn	Knudsen number
L	Characteristics length (m)
m	Mass flow rate (kg s^{-1})
P	Pressure (pa)
ΔP	Pressure drop (pa)
P_p	Pumping power (W)
q	Heat generation (W)
Q	Volumetric flow rate ($\text{m}^3 \text{s}^{-1}$)
Re	Reynolds number
R_t	Thermal resistance (K/W)
T	Temperature ($^\circ\text{C}$)
v	Velocity (ms^{-1})
X, Y, Z	Cartesian coordinates

Greek symbols

Ψ	Sphericity
ρ	Density (kg m^{-3})
μ	Viscosity ($\text{m}^2 \text{s}^{-1}$)
γ	Nanoparticles diameter
λ	Mean free path
φ	Particle volume fraction

Subscripts

f	Fluid
in	Inlet fluid
max	Maximum
nf	Nanofluid
ov	Overall
out	Outlet fluid
pw	Pure water
s	Solid

E. Farsad (✉) · S. P. Abbasi · M. S. Zabihi · J. Sabbaghzadeh
Iranian National Center for Laser Science
and Technology, Tehran, Iran
e-mail: ehsanfarsad@yahoo.com; farsad@nlc.ir

v_{avg} Volume average
 w Top wall of MCHS (heated surface)

1 Introduction

One of the most critical issues in the electronic industry is the thermal management of electronic devices, especially meeting the limitations on maximum operating temperature and ensuring temperature uniformity across the devices. These factors directly affect the performance, cost, and reliability of electronic devices. A review of recent literature clearly indicate growing demand for reducing the volume and weight of electronic devices while increasing their complexity and power density for numerous applications including computers, automotive, and aerospace. Currently, the major limitation for the development of more compact electronic and MEMS devices is due to the lack of an efficient technique to remove heat from these devices.

A significant progress has been made in the past two decade to fabricate micro devices with novel micro structures and increased integration of electronics. This development has created a need for improved cooling technologies to achieve high heat dissipation rates for these high power density microelectronic components. In the area of thermal science this development has caused a shift in thermal phenomena from macro scale to micro and nano scales.

The increased integration and compact electronics has led to challenges for the thermal design, development, packaging and assessment of innovative high performance cooling techniques. Future micro electronic components are projected to dissipate over $1,000 \text{ W/cm}^2$ and these high heat fluxes cannot be easily dissipated using existing cooling techniques [1].

In recent years, efforts have been made to develop cooling devices as integrated parts of the electronics [2–4]. Several possible cooling solutions, including two phase flow, nucleate boiling, microchannel heat sinks, nanofluids and jet impingement; have recently been investigated by various authors [5–7]. Among the cooling methods, the microchannel heatsink has been proven to be a high performance cooling method.

Early in 1981, Tuckerman and Pease presented the first micro channel heat sink with parallel micro channels etched in silicon substrate [8]. The MCHS has received extensive study over the past two decades because of its capability to dissipate large amounts of heat from a small area [9–11].

The most frequently used coolants in the MCHS were air, water and fluoro-chemicals. The heat transfer capability is limited by the base fluid transport properties. Water possesses the highest thermal conductivity among all the fluids

we use today, though it amounts to merely 0.6 W/mK under room temperatures, which is several orders lower than most metals or metal oxides. It would perhaps be logical to add certain solid particles into a base liquid to increase its thermal conductivity k , a concept that has been practiced for a long time. Most of these early studies, however, used suspensions of millimeter or micrometer sized particles, which led to problems such as poor suspension stability and hence channel clogging, often serious for systems consisting of small channels. Nanofluids are dilute suspensions of functionalized nanoparticles smaller than 100 nm , which belong to a new type of functional composite materials developed about a decade ago with the specific aim of increasing the thermal conductivity of heat transfer fluids [12]. There have been relatively few studies on nanofluid flow and heat transfer characteristics as comparing with those of pure fluid in practical applications [13]. These studies indicated that the heat transfer coefficient was greatly enhanced in the nanofluid flow. The enhancement depended on the Reynolds flow number, particle Peclet number, particle size, shape and particle volume fraction. They also found that nanoparticles did not cause an extra pressure drop in the flow. Using nanofluids as a coolant in the microchannel heatsink could further improve its performance.

Chein and Huang [14] analyzed the performance of the MCHS using a Cu–water nanofluid with $\phi = 0.3\text{--}2\%$. The Nusselt number increased significantly with an increase in Re and ϕ . The maximum reduction in thermal resistance as compared to pure water was found to be 15% at $\phi = 2\%$ and power = 3 W . The additional reduction in R_t is clearly due to thermal dispersion.

Koo and Kleinstreuer [15] simulated and analyzed the Conduction convection heat transfer of nanofluid (CuO–water and ethylene glycol, $\gamma = 20 \text{ nm}$) in a rectangular microchannel ($50\text{--}300 \mu\text{m}$). The Nusselt number for ethylene glycol based nanofluids was always higher than for water based ones, due to stronger thermal flow development effects. Moreover, the viscous dissipation effect was found to affect only ethylene glycol based nanofluids and was more important for flows through very narrow channels.

Jang and Choi [16] numerically investigated the cooling performance of a silicon microchannel heat sink under forced convective flow with nanofluid Cu–water and diamond–water; for $\phi = 1\%$. The nanofluids reduced the thermal resistance of the heat sink and enhanced the cooling performance by 4 and 10% , respectively. Further, the potential of employing a microchannel heat sink with nanofluid to remove ultra high heat flux as much as $1,350 \text{ W/cm}^2$ when the difference between the junction temperature and inlet coolant temperature is 80°C , was demonstrated.

Chein and Chuang [17] used a nanofluid (CuO–water, $\phi = 0.204, 0.256, 0.294$ and 0.4%) with 80 nm long and

20 nm wide particles. The energy absorbed by the nanofluid was greater than that absorbed by water and was found to increase with the increase in particle volume fraction. A large temperature difference between the MCHS inlet and outlet was obtained at a low flow rate. Although the nanofluids had higher viscosity, only a minimal increase (around 5%) in the pressure drop across the MCHS was reported.

Wang and Ding [18] numerically simulated the three-dimensional fluid flow and heat transfer process in a newly introduced microchannel heat sink and the conventional microchannel heat sink. It was found that the temperature rise along the flow direction decreases significantly in the new microchannel heat sink resulting from the entrance effects in the transverse channel arrays, which is proved by much higher heat flux values obtained near the transverse channel array inlet.

Ho and Wei [19] experimentally investigated forced convective cooling performance of a copper MCHS with $\text{Al}_2\text{O}_3/\text{water}$ nanofluid as the coolant. They used a microchannel heatsink fabricated consists of 25 parallel rectangular microchannels of length 50 mm with a cross sectional area of $283 \mu\text{m}$ in width by $800 \mu\text{m}$ in height for each microchannel. Results showed that the nanofluid cooled heat sink outperforms the water cooled one, having significantly higher average heat transfer coefficient and thereby markedly lower thermal resistance and wall temperature at high pumping power, in particular.

In most of the studies mentioned above, focus on the regular geometry of MCHS with rectangular channels. This work presents a micro channel heatsink in a novel geometric configuration. This MCHS appears to be a viable solution to high heat rejection requirements of today's high power electronic devices. In addition, we show that a novel combination of a micro channel heatsink with nanofluids as a new coolant gives a new direction for removing ultra high heat flux as much as $2,000 \text{ W/cm}^2$, when the difference between junction temperature and inlet coolant temperature is 80°C . For this purpose, a three-dimensional computational fluid dynamics model is developed using the commercial software package FLUENT, to investigate the conjugate fluid flow and laminar forced convective heat transfer characteristics of $\text{Al}_2\text{O}_3/\text{water}$, CuO/water and Cu/water nanofluids as coolants flowing in a copper MCHS. The temperature distribution details, thermal resistance and pumping power of microchannel heatsink with nanofluids as compared to pure water will be discussed.

2 Description of microchannel heatsink

A schematic representation of the irregular microchannel heat sink is shown in Fig. 1. It consists of five copper sheets with 0.4 mm thickness, which are manufactured by

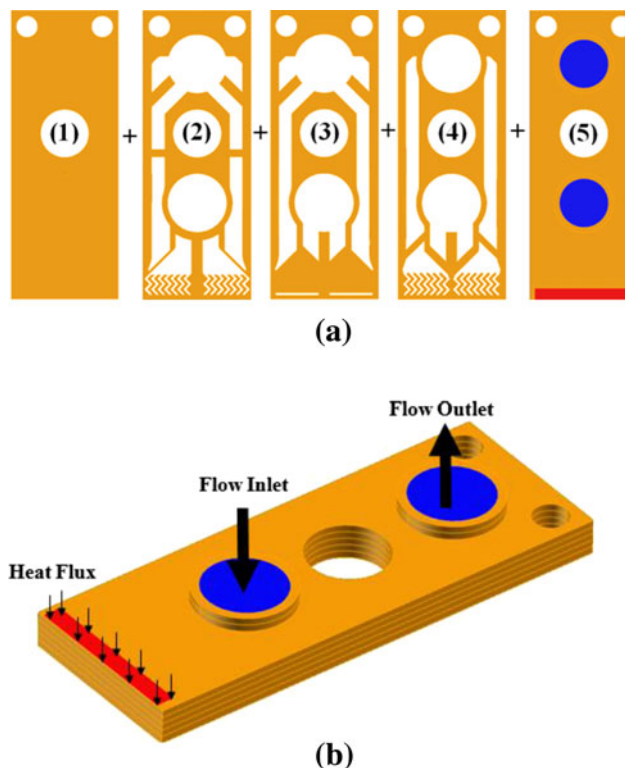


Fig. 1 Schematic of MCHS **a** an exploded view of five sheets of MCHS, **b** the isometric view of MCHS

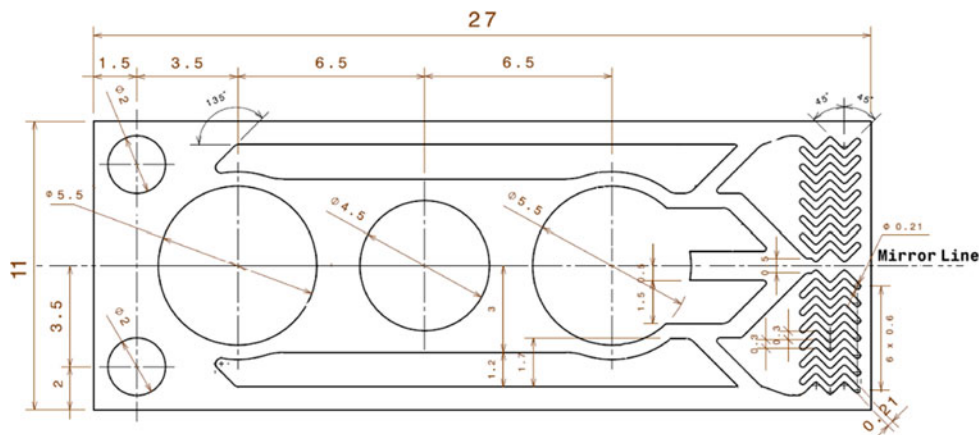
micro machining and joined by diffusion bonding. The overall dimensions of the MCHS are $27 \times 11 \text{ mm}$ with 2 mm thickness (Fig. 1b). The top sheet (Fig. 1a) of the MCHS contains the coolant inlet and outlet. The zig zag channels consist of 14 channels on the second and fourth sheet (Fig. 1a). The bottom sheet (first sheet) acts as sealing cover. Once the nanofluid enters the zig zag channels in second sheet, passes the rectangular channel in third sheet. Then nanofluid enters the zig zag channels in fourth sheet and receives uniform heat flux from electronic device which is conducted to the top surface of MCHS and exits from outlet of MCHS (Fig. 1b). The dimensions of fourth sheet of MCHS are shown in Fig. 2.

3 Numerical modeling

3.1 Assumptions

The nanoparticles in the base fluid may be easily fluidized and consequently the effective mixture behaves like a single phase fluid [20]. It is also assumed that the fluid phase and nanoparticles are in thermal equilibrium with zero relative velocity. Under these assumptions, the classical theory of single phase fluid can be applied to nanofluids.

Fig. 2 The dimensions of fourth sheet of MCHS, (unit:mm)



The hydraulic diameter of the microchannel is about 275 μm . This yields a typical Knudsen number ($\text{Kn} = \lambda/L$) for nanofluid, as a coolant, which lies in the continuous flow regime [21]. Therefore, the conservation equations based on the continuum model (Navier–Stokes equations of motion) can still be used to describe the transport processes.

3.2 Governing equations

A modified single phase model accounting for thermal dispersion has been used for the simulation of laminar forced convective heat transfer characteristics of nanofluid flowing in a microchannel heatsink. Heat transfer process in the MCHS is a conjugate problem that combines heat conduction in the solid and convective heat transfer to the cooling fluid. Some simplifying assumptions are required when the commercial software package (FLUENT) is used to solve governing equations of the heat transfer process in the analysis MCHS. The major assumptions are:

1. Steady fluid flow and heat transfer
2. Incompressible fluid
3. Laminar flow
4. Constant solid and fluid properties
5. Negligible radiation.

The complete set of governing equations for this 3D conjugate heat transfer problem in micro scale dimensions using thermal dispersion model are given below using Eqs. 1–5. The continuity equation for nanofluid zone is written as:

$$\nabla \cdot v = 0 \quad (1)$$

The momentum conservation equation:

$$\rho_{nf} v \cdot \nabla v = -\nabla p + \nabla \cdot (\mu_{nf} \nabla v) \quad (2)$$

The energy equation for nanofluid zone:

$$\rho_{nf} C_{p,nf} v \cdot \nabla T = k_{nf} \nabla^2 T \quad (3)$$

For the solid, the momentum equation:

$$\nabla \cdot v = 0 \quad (4)$$

In addition, the energy equation is:

$$\nabla \cdot (k_s \nabla T) = 0 \quad (5)$$

3.3 Boundary conditions

The governing equations of the fluid flow are non-linear and coupled partial differential equations that must be solved subject to appropriate boundary conditions outlined below:

1. At the inlet, uniform velocity and temperature is specified so as to consider the development of velocity and temperature field. Therefore it assumes fully developed flow at inlet.
2. Outflow boundary condition has been specified at the microchannel outlet.
3. Uniform heat flux specified as a boundary condition at the heated top wall of the MCHS while all other walls are perfectly insulated.
4. Coupled thermal boundary condition was chosen for all solid–fluid interfaces in this 3D conjugate heat transfer problem. This enforces continuity of temperature and heat flux at solid–liquid interfaces as in Eqs. 6–7:

$$T_s = T_{nf} \quad (6)$$

$$k_s \frac{\partial T_s}{\partial n_s} = k_{nf} \frac{\partial T_{nf}}{\partial n_{nf}} \quad (7)$$

5. Only half of the microchannel heatsink is modeled due to the symmetry.

3.4 Thermophysical properties

In this study, the $\text{Al}_2\text{O}_3/\text{water}$, CuO/water and Cu/water nanofluids are to be used as the working fluid. The

thermophysical properties involved in the governing equations are replaced by those of the nanofluid. That is $\rho_f, (\rho c_p)_f, \mu_f, k_f$ are to be replaced by $\rho_{nf}, (\rho c_p)_{nf}, \mu_{nf}, k_{nf}$, respectively. The density and specific heat capacity of nanofluid are given as [20]:

$$\rho_{nf} = (1 - \varphi)\rho_f + \varphi\rho_s \quad (8)$$

$$(\rho c_p)_{nf} = (1 - \varphi)(\rho c_p)_f + \varphi(\rho c_p)_s \quad (9)$$

The effective viscosity of nanofluid as in using Einstein's equation is given as [22]:

$$\mu_{nf} = \mu_f(1 + 2.5\varphi) \quad (10)$$

The effective thermal conductivity of nanofluid is given as [22]:

$$k_{nf} = k_f + 3\Psi^{-1}\varphi \frac{k_s - k_f}{(3\Psi^{-1} - 1)k_f + k_s - \varphi(k_s - k_f)} \quad (11)$$

Thermophysical properties of nanofluid is related to the particle volume fraction which is defined as the fraction of volume occupied by particle in a unit volume of bulk fluid, as shown in Eqs. 8–11. The density and specific heat capacity of nanofluid are simply evaluated based on the volume fractions of each phase composed of nanofluid. In recent years, there have been many researches devoting into evaluating the thermal conductivity of nanofluid [12, 13]. Because the nanofluid can be made using large varieties of nanoparticles, base fluid, particle shape and particle volume fractions, the results from these studies show a large variety in nanofluid thermal conductivity. Equation 11 is regarded as the theoretical model for the nanofluid thermal conductivity proposed by Hamilton and Crosser [22] based on treating nanofluid as liquid–solid mixture for static suspension. In addition to the thermal conductivity of the particle and fluid, the thermal conductivity of the nanofluid under static conditions also depends on the shape factor of the nanoparticles which is given as Ψ is the sphericity defined as the ratio of the surface area of a sphere with a volume equal to that of the particle to the surface area of the particle. Recent studies indicated that Eq. 11 underestimates the thermal conductivity of oxide nanofluid [23]. Therefore in this paper, thermal conductivity of Al_2O_3 /water nanofluid is calculated from the correlation developed by Li and Peterson [24]. They used a steady state method called the cut bar method for the measurement of thermal conductivity. They found a huge effect of temperature on the thermal conductivity of Al_2O_3 and CuO based nanofluids with water as the base fluid. Based on their observations, they suggested the following equations for thermal conductivity enhancement, obtained by linear regression analysis for Al_2O_3 /water nanofluids:

$$\frac{k_{nf} - k_f}{k_f} = 0.7645\varphi + 0.01869T - 0.4621 \quad (12)$$

For CuO/water nanofluids, the equation is:

$$\frac{k_{nf} - k_f}{k_f} = 3.761\varphi + 0.0179T - 0.3073 \quad (13)$$

Therefore, in our simulations the thermal conductivity of oxide nanofluid is temperature dependent. The properties of solid particles and base fluid are taken to be constant in operating temperature range of 22°C to about 30°C because the variations of the base fluid properties are <1% in the operating temperature range. The Thermophysical properties are listed in Table 1 [25].

3.5 Numerical method

The set of governing Eqs. 1–5 with boundary conditions described in Sect. 3.3 has been solved using finite volume approach. This approach is based upon spatial integration of the governing equations over finite control volumes. Commercial CFD software package FLUENT ver 6.3.26 has been used for the simulation. The discretization software Gambit ver 2.3.16 was used for meshing the micro channel heatsink using the TGrid type with tetrahedron and hybrid volume elements. Figure 3 depicts the finite volume mesh of the half of MCHS with 17.13×10^5 cells. Steady state 3D segregated solver has been used. Conjugate boundary condition at solid–fluid interfaces ensures that energy equation in solid and fluid zones are solved simultaneously. Temperature dependence of thermal conductivity of oxide

Table 1 Thermophysical properties of nanoparticles and base fluid at 300 K [25]

Properties	Nanoparticles			Base fluid
	Al_2O_3	CuO	Cu	Water
ρ	3,880	6,510	8,933	997
C_p	729	540	385	4,170
K	42.34	18	401	0.613
μ	–	–	–	0.855E–3

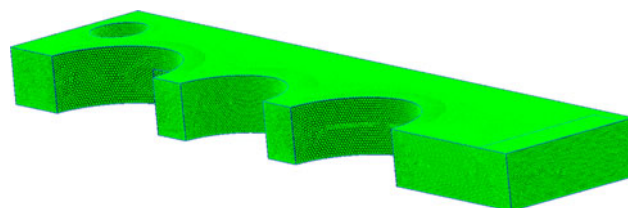


Fig. 3 The finite volume mesh of the half of the MCHS

nanofluid has been incorporated in the model using User-defined function (UDF). Semi-implicit method for pressure-linked equations (SIMPLE) algorithm has been used for pressure–velocity coupling whereby continuity and momentum equations are combined to derive pressure-correction equation. The pressure is discretized by using the standard scheme. Second order upwind scheme has been used to discretize the advective terms in momentum and energy equations to contain numerical errors. Entire domain was initialized with the conditions of inlet boundary before starting the iterative process. Under relaxation factors for the update of computed variables at each iteration are for pressure = 0.3, momentum = 0.3 and energy = 1. Qualitative convergence has been obtained by energy residual falling below 10^{-7} , continuity below 10^{-3} and velocity components below 10^{-3} .

3.6 Mesh independence and simulation validation

The numerical simulation is verified in a number of ways to ensure the validity of the numerical analysis. The grid dependence test is first conducted by using several different mesh sizes. Figure 4 shows the variation of temperature along the length of MCHS. The deviation between low mesh size (mesh size 290,680) and medium mesh size (mesh size 368,747) is significant, while the deviation between high mesh sizes (mesh size 403,944 and 437,496) is very small. Hence based on these results, it is decided to use high mesh size (mesh size 403,944) in all calculations.

The numerical simulation was validated with the results of Dix [26]. Figure 5 compares the surface temperature

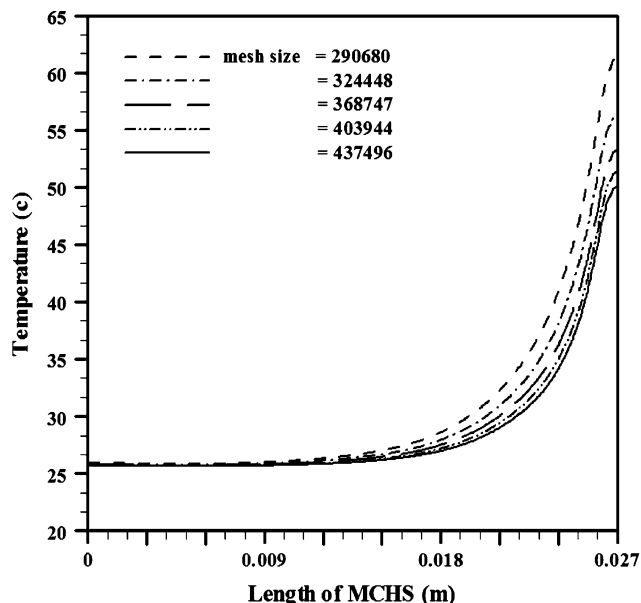


Fig. 4 Variation of temperature along the length of MCHS for five different mesh sizes

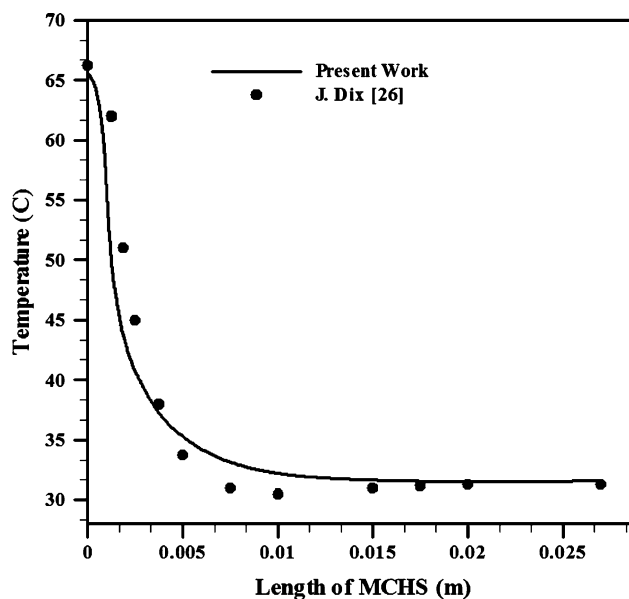


Fig. 5 Comparison among the simulation results and the results of Dix [26] for surface temperature profile

profile along the length of MCHS, as numerical results with the numerical data [26]. The surface temperature profile obtained from the present work and numerical results in the MCHS with pure water at same initial conditions was found to overlap along the length of MCHS. Therefore the validating of the numerical simulation is demonstrated.

4 Results and discussions

The numerical analysis was performed for the irregular micro channel heat sink and the results are presented in this section. Some important input conditions for simulation that are employed in this study are summarized in Table 2. The wall temperature and the temperature distribution of MCHS are presented first.

Table 2 Input conditions for simulation

Coolant	Al ₂ O ₃ /Water
Inlet fluid temperature	22 (°C)
Inlet fluid pressure	1 (bar)
Volumetric flow rate	0.3 (l/min)
Inlet fluid velocity	0.212 (m/s)
Concentration of nanoparticles	0, 2, 4, 6, 8 vol%
Nanoparticles diameter	11 nm
Heat flux	1,237 (w/cm ²)
Heated surface area	Width: 9.7 mm (Y direction) Length: 1 mm (X direction)
Material of MCHS	Copper

4.1 Wall temperature

An important design feature is the temperature variation on the top (heated) surface of the MCHS. A low and uniform temperature on this surface is preferable in order to avoid hotspots on the micro electronic devices, resulting in damage, failure, or incorrect data. Figure 6 shows the magnitude of the wall temperature maximum ($T_{w,max}$) decreases 2.3% by about 8% vol for Al_2O_3 nanofluid compared with the

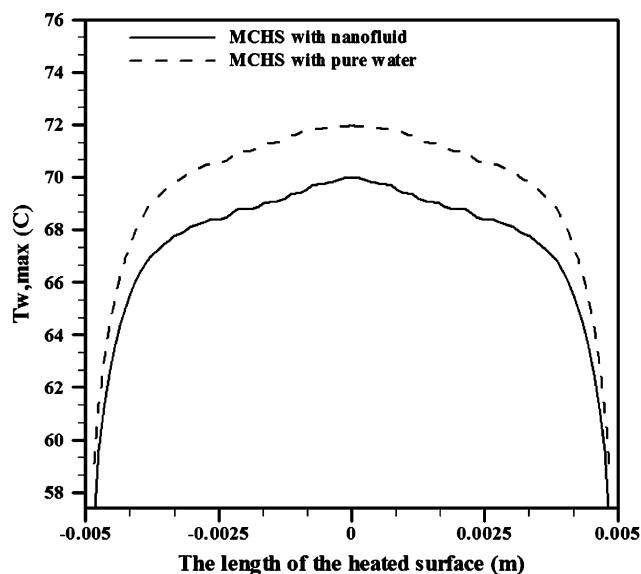


Fig. 6 The maximum of the wall temperature along the length of the heated surface

microchannel heatsink with pure water because the thermal conductivity of nanofluid is larger than the water. Thus, when the temperature difference between wall temperature an inlet coolant temperature (base input condition) is $80^{\circ}C$ [16], heat flux of up to $2,000\text{ W/cm}^2$ can be dissipated by a microchannel heatsink with Al_2O_3 nanofluid (8% vol) at pumping power 0.9 W. We can purpose a MCHS with nanofluids as a next generation cooling devices for removing ultra-high heat flux of microelectronic components.

The temperature difference distribution between heated wall an inlet coolant at X–Y plane of MCHS with nanofluid Al_2O_3 (8% vol) compared with pure water is illustrated in Fig. 7a, b. From the distribution of constant temperature contour lines, the temperature difference of MCHS with nanofluid is more uniform than the MCHS with pure water. A high temperature difference is found in the edge of MCHS at y middle plane, where $y = 0$ and $x = 1$ mm. Because there is not zigzag channel in the solid region for cooling under this point. This difference decreases from the edge of MCHS to the region near the channel inlet where $x = 0$ mm.

4.2 Temperature distribution of MCHS

Based on the numerical results, Fig. 8 shows colored temperature contours of the top view of micro channel heatsink with pure water and water based nanofluids containing Al_2O_3 with 8% volume fraction under the input conditions that were listed in Table 2. Figure 8a shows that, when water is used as the coolant, there is a large region of red, indicating the temperature of MCHS greater

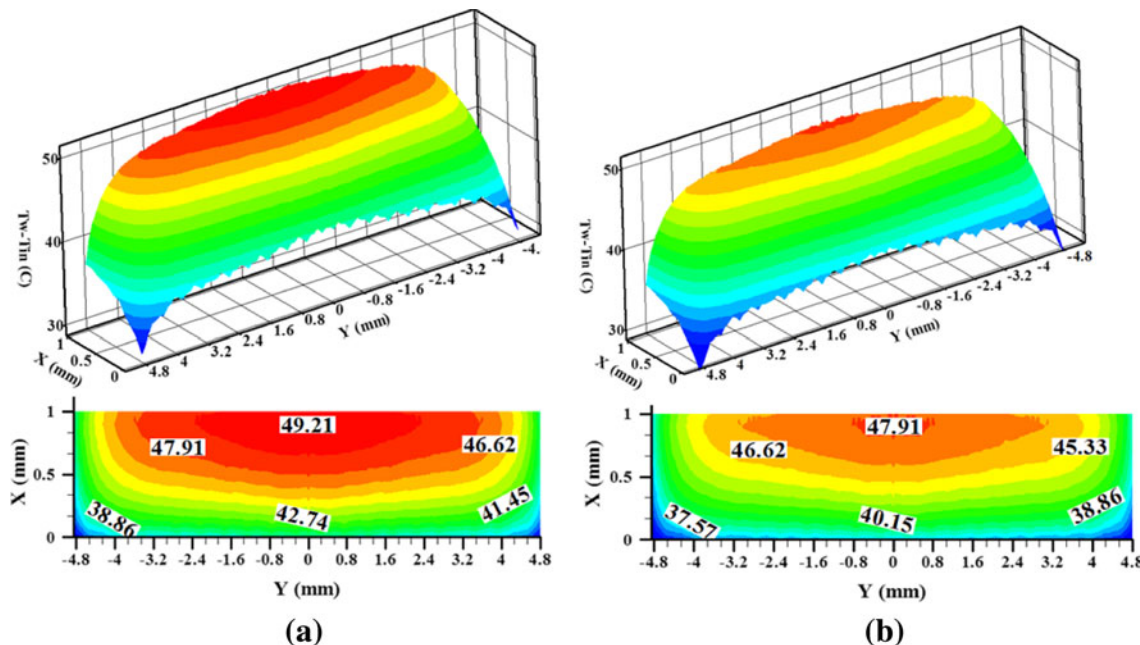


Fig. 7 The temperature difference distribution between heated wall an inlet coolant at X–Y plane: MCHS with a pure water, b Al_2O_3 nanofluid (8% vol.)

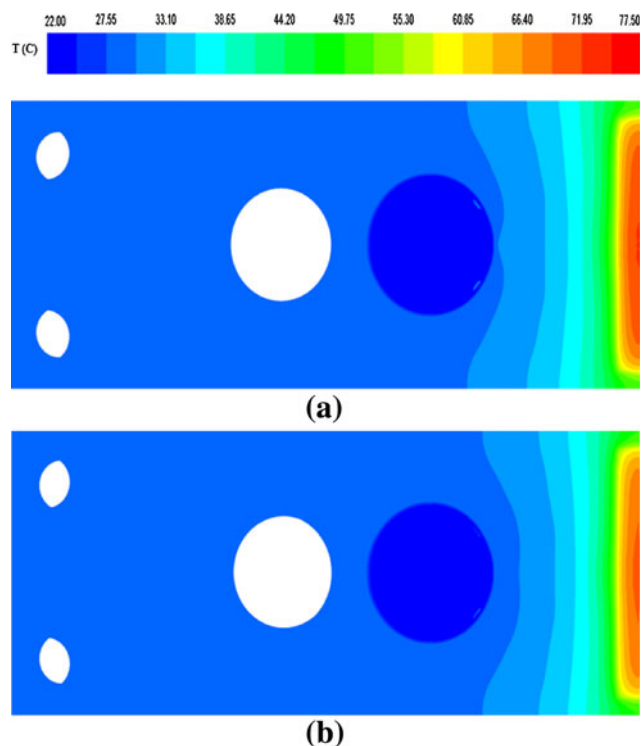


Fig. 8 Temperature contours for top view of MCHS: **a** with pure water, **b** with Al_2O_3 (8% vol.)

than 71°C . However this deep red region shrinks for water-based nanofluid containing Al_2O_3 (8% vol.) as shown in Fig. 8b. The colored contour maps are a powerful way to visually examine the cooling performance of different coolants flowing in the MCHS. As shown in Fig. 8 the uniformity of temperature in the MCHS is enhanced by using nanofluids because the thermal conductivity of nanofluids is larger than that of pure water. Hence this uniformity of temperature causes the thermo mechanical stresses between MCHS and micro electronic devices reduce and the lifetime of devices increases.

4.3 Parametric studies

4.3.1 Effects of nanoparticles concentration

The effects of nanoparticles concentration on convective heat transfer augmentation in MCHS are listed in Table 3.

Table 3 shows that the wall temperature maximum reduces by about 1% as Al_2O_3 nanoparticles concentration is increased from 2 to 8% vol. It is clear that the augmentation of nanoparticles concentration which causes volume average of the nanofluid thermal conductivity increases 4.5%. So the heat transfer rate of nanofluid increases and the wall temperature decreases.

Pumping power (P_p) is needed to drive the working fluid in microchannels, which is defined as the product of the pressure drop across the channel (ΔP) and volumetric flow rate (\dot{Q}), i.e.,

$$P_p = \Delta P \dot{Q} \quad (14)$$

Based on the numerical results, Table 3, there is not difference in pumping power when using pure water and nanofluids. There is an average 5% increase for Al_2O_3 nanofluid with a 2% volume fraction and an average 11% enhancement for the Al_2O_3 nanofluid with a 4% volume fraction compared with pure water. Thus, it does not need additional pumping power to drive nanofluid flow, especially, for lower particle volume fractions.

The cooling performance of a microchannel heat sink with nanofluids is evaluated by the overall thermal resistance, $R_{t,ov}$ defined as:

$$R_{t,ov} = \frac{T_{w,max} - T_{nf,in}}{q} \quad (15)$$

where q , $T_{w,max}$ and $T_{nf,in}$, are the heat added to the MCHS, the wall maximum temperature and the inlet coolant temperature, respectively.

Table 3 shows that nanofluid reduce the thermal resistance, as defined by Eq. 15. The numerical results indicate that the cooling performance of MCHS is enhanced by about 4.5 and 2.4% for Al_2O_3 nanofluid with 8 and 2% volume fraction respectively, compared with micro channel heatsink with pure water.

4.3.2 Effects of volumetric flow rate

The effects of volumetric flow rate on force laminar convective heat transfer in the micro channel at a fixed nanoparticles concentration of 8% volume fraction are listed in Table 4. The inlet fluid temperature and the heat flux supplied to the heat sink top wall are kept constant in

Table 3 Simulation results

Case no.	ϕ	$T_{w,max}$	$T_{nf,max}$	$T_{nf,vavg}$	$R_{t,ov}$	ΔP	P_p	$K_{nf,vavg}$	$h_{nf,vavg}$
1	0	72.34	60.35	27	0.42	147,904	0.74	0.613	951.5
2	2	70.69	59.52	27	0.41	155,290	0.778	0.649	961
3	4	70.51	59	27	0.405	164,574	0.82	0.659	963
4	6	70.33	58.88	27	0.402	172,608	0.86	0.668	966
5	8	70.16	58.7	27	0.401	180,916	0.91	0.678	968

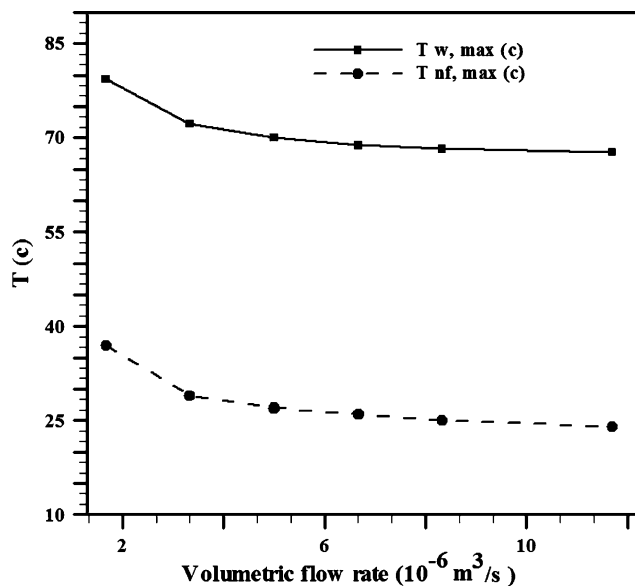
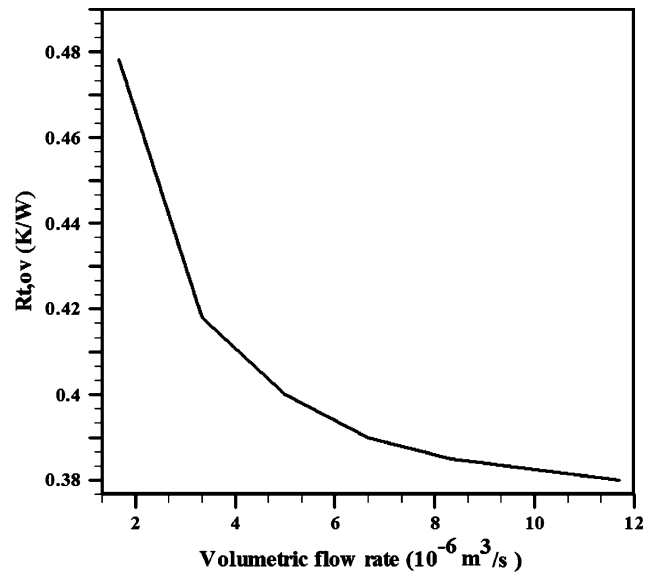
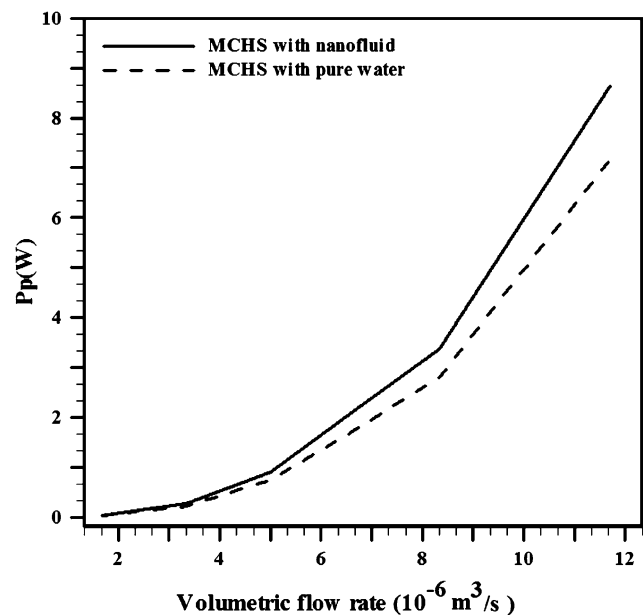
Table 4 Simulation results of the effects of volumetric flow rate

Case no.	\dot{Q} ($\times 10^{-6}$)	$T_{w,max}$	$T_{nf,vavg}$	$V_{nf,vavg}$	$R_{t,ov}$	P_p (W)	$K_{nf,vavg}$	$h_{nf,vavg}$
1	1.67	79.38	37	0.64	0.478	0.035	0.794	696
2	3.33	72.23	29.6	1.29	0.418	0.268	0.707	881
3	5	70	27	1.96	0.400	0.900	0.678	968
4	6.67	68.8	26	2.63	0.390	2.150	0.663	1,019
5	8.33	68.23	25	3.3	0.385	3.370	0.655	1,054
6	11.7	67.7	24	4.61	0.38	8.64	0.645	1,098

the cases studies. Figure 9 shows the effects of flow rate augmentation on the maximum wall temperature and volume average of fluid temperature of MCHS with Al_2O_3 nanofluid. It can be seen that the maximum wall temperature and fluid temperature reduce with increasing flow rate. Reduction of temperatures can be attributed to higher fluid average velocity (Table 4) as well as increased thermal dispersion effect. The temperatures gradients are more at low flow rate because the thermal dispersion effect is negligible.

Figure 10 depicts the effects of flow rate on overall thermal resistance. It reduces about 9% as flow rate is increased from 3.33×10^{-6} to $11.7 \times 10^{-6} m^3/s$ at MCHS with nanofluid. Reduction of thermal resistance can be attributed to higher flow rate as well as increased thermal dispersion effects.

Figure 11 shows the effects of flow rate augmentation on the pumping power of MCHS with Al_2O_3 nanofluid and pure water. It can be seen that the pumping power increases with increasing flow rate. Increasing of the pumping power

**Fig. 9** Effect of flow rate on wall temperature and volume average of nanofluid temperature**Fig. 10** Effect of flow rate on overall thermal resistance**Fig. 11** Effect of flow rate on pumping power of MCHS with nanofluid and pure water

can be attributed to higher fluid average velocity as well as increased pressure drop across the MCHS.

The augmentation of pumping power is more apparent at high flow rate because the pressure drop is proportional to the square of fluid volume average velocity as follows:

$$\Delta P = v_{nf,avg}^2 \quad (16)$$

Figure 12 depicts the effects of flow rate on volume average of nanofluid thermal conductivity. Nanofluid thermal conductivity reduces about 8.8% as flow rate is

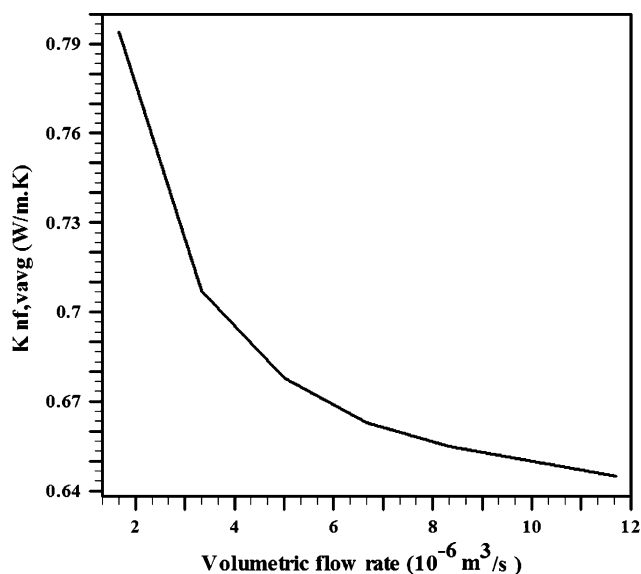


Fig. 12 Effects of flow rate on nanofluid thermal conductivity

increased from 3.33×10^{-6} to $11.7 \times 10^{-6} \text{ m}^3/\text{s}$. In our simulations the thermal conductivity of oxide nanofluids are temperature dependent (Eq. 12). Hence, Reduction of nanofluid thermal conductivity can be attributed to higher flow rate as well as decreased volume average of nanofluid temperature.

Figure 13 shows the effects of flow rate on the volume average of the nanofluid surface heat transfer coefficient (SHTC). The augmentation of the flow rate causes thermal dispersion increases so the surface heat transfer coefficient of fluid increases.

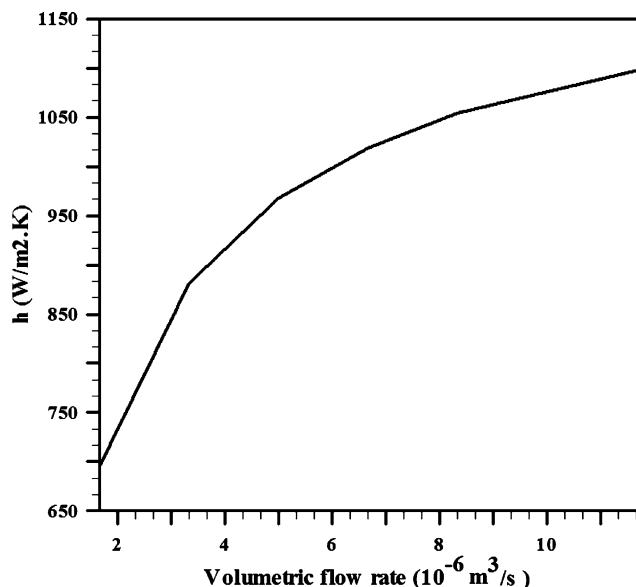


Fig. 13 Effects of flow rate on nanofluid SHTC

4.3.3 Effects of various nanoparticles

The effects of various nano particle on the performance of micro channel at a fixed nanoparticles concentration of 4% volume fraction are listed in Table 5. The inlet fluid temperature, the heat flux supplied to the heat sink top wall and the volumetric flow rate are kept constant. In this section for a just comparison between various nanoparticles, the thermal conductivity of nanofluid with various nanoparticles is taken to be constant in the present operating temperature range.

Table 5 shows the overall thermal resistance of MCHS with nanofluid containing Cu increases about 8.4 and 9.6% compared that at MCHS with containing Al_2O_3 and CuO, respectively. Hence the cooling performance of a micro channel heat sink with metal nanofluids improves compared with that of a micro channel heat sink with oxide metal nanofluids.

Base on the numerical results, Fig. 14 shows the temperature difference distribution between heated wall an inlet coolant at X–Y plane of MCHS with various nanoparticles is illustrated in Fig. 14a–c).

From the distribution of constant temperature contour lines, the temperature difference of MCHS with nanofluid containing Cu (Fig. 14c) is lower and more uniform than the MCHS with Al_2O_3 and CuO. It can be attributed the thermal conductivity of Cu nanofluid is larger than that of Al_2O_3 and CuO at 4% volume fraction (Table 5).

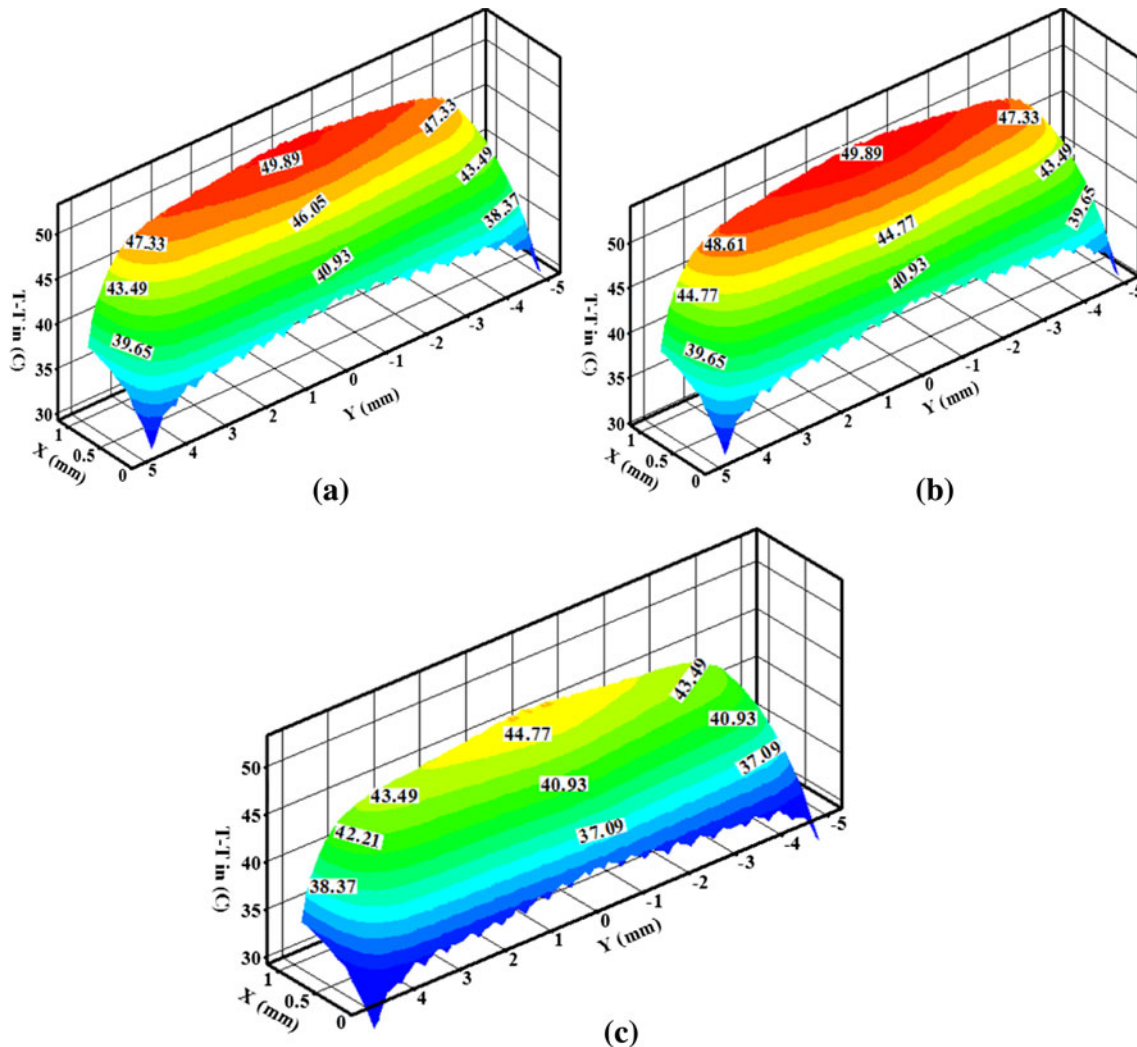
5 Conclusion

This study presented a microchannel heatsink in a novel configuration with nanofluid as the coolant. This MCHS with nanofluid appeared to be good candidates as the next generation cooling devices for removing ultra high heat flux of today's high power electronic devices. In the present work, three-dimensional fluid flow and conjugate laminar forced convective heat transfer characteristics of $\text{Al}_2\text{O}_3/\text{water}$, CuO/water and Cu/water nanofluids as coolants flowing in a copper microchannel heatsink with zigzag channels in a novel irregular geometric configuration were analyzed numerically.

A detailed description of the local and volume average of heat transfer characteristics, i.e., temperature, overall thermal resistance, volumetric flow rate, thermal conductivity, pumping power and surface heat transfer coefficient was obtained. The effects of nanoparticles concentration, volumetric flow rate of coolant and various nanoparticles on the cooling performance of MCHS were presented and discussed. The following conclusion can be drawn from the present results:

Table 5 Simulation results of the effects of nanoparticles material

Case no.	\dot{Q} ($\times 10^{-6}$)	Nanoparticle	$T_{w,max}$	$T_{nf,vavg}$	$R_{t,ov}$	P_p (W)	K_{nf} [15]	$h_{nf,vavg}$
1	3.33	Al_2O_3	72.2	29	0.417	0.28	0.668	893
2	3.33	CuO	72.8	29.48	0.423	0.27	0.699	894
3	3.33	Cu	67.9	29	0.382	0.29	1.024	970

**Fig. 14** Temperature difference distribution between heated wall and inlet coolant at X–Y plane: MCHS with **a** Al_2O_3 nanofluid, **b** CuO nanofluid, **c** Cu nanofluid

1. The highest temperature point is located at the heated base surface of the MCHS, which is in the edge of MCHS at y middle plane, where $y = 0$ and $x = 1$ mm. Because there is not zigzag channel in the solid region for cooling under this point.
2. $T_{w,max}$ decreases 3% by about 8% volume fraction for Al_2O_3 nanofluid compared with that of the MCHS with pure water because the thermal conductivity of nanofluid is larger than that of water.
3. The wall temperature maximum reduces by about 1% as Al_2O_3 nanoparticles concentration is increased from 2 to 8% vol.
4. The potential of developing a combined micro channel heatsink with nanofluids as the next generation cooling devices for removing ultra high heat flux as much as $2,000 \text{ W/cm}^2$, when the difference between junction temperature and inlet coolant temperature is 80°C .

5. The uniformity of temperature in the MCHS is enhanced by using nanofluids. Therefore, this uniformity causes the thermo mechanical stresses between MCHS and microelectronic devices reduce.
6. Increasing flow rate reduces the wall temperature maximum, fluid temperature and overall thermal resistance. Reduction of these parameters can be attributed to higher fluid average velocity as well as increased thermal dispersion effects.
7. The cooling performance of a micro channel heat sink with metal nanofluids improves compared with that of a micro channel heat sink with oxide metal nanofluids because the thermal conductivity of metal nanofluid is higher than oxide metal nanofluids.

References

1. Linan J, Jae MK, Evelyn W (2002) Cross-linked microchannels for VLSI Hotspot cooling. In: Proceedings of IMECE 2002, ASME, New York, pp 1–5
2. Bjorn P (1996) Cooling of electronics by heat pipes and thermosyphons. In: National heat transfer conference, vol 329(7). ASME, New York, pp 97–108
3. Jiang L, Wong M (1999) Phase change in micro channel heat-sinks with integrated temperature sensors. *J Microelectromech Syst* 8(4):358–365
4. Evelyn NW, Lian Z (2002) Micro machined jet arrays for liquid impingement cooling of VLSI chips, Solid-State Sensor, Actuator and Micro systems workshop, Hilton head island, pp 46–49
5. Lee J, Mudawar I (2005) Two-phase flow in high heat flux micro channel heat sink for refrigeration cooling applications: part I: pressure drop characteristics. *Int J Heat Mass Transf* 48:928–940
6. Ghajar M, Darabi J (2005) Numerical modeling of evaporator surface temperature of a micro loop heat pipe at steady-state condition. *J Micromech Microeng* 15:1963–1971
7. Zhuan R, Wang W (2010) Simulation on nucleate boiling in micro-channel. *Int J Heat Mass Transf* 53:502–512
8. Tuckerman DB, Pease RFW (1981) Pease, High-performance heat sinking for VLSI. *IEEE* 2:126–129
9. Qu W, Mudawar I (2002) Experimental and numerical study of pressure drop and heat transfer in a single-phase micro-channel heat sink. *Int J Heat Mass Transf* 45:2549–2565
10. Li J, Peterson GP (2004) Three-dimensional analysis of heat transfer in a micro-heat sink with single phase flow. *Int J Heat Mass Transf* 47:4215–4231
11. Jung JY, Kwak HY (2008) Fluid flow and heat transfer in micro channels with rectangular cross section. *Heat Mass Transf* 44:1041–1049
12. Choi S, Singer DA, Wang HP (1995) Enhancing thermal conductivity of fluids with nanoparticles, in developments and applications of non-Newtonian Flows, FED 231. ASME, New York, pp 99–105
13. Wen D, Lin G, Vafaei S, Zhang K (2009) Review of nanofluids for heat transfer applications. *Particology* 7:141–150
14. Chein R, Huang G (2005) Analysis of microchannel heat sink performance using nanofluids. *Appl Therm Eng* 25:3104–3114
15. Koo J, Kleinstreuer C (2005) Laminar nanofluid flow in micro heat-sinks. *Int J Heat Mass Transf* 48:2652–2661
16. Jang SP, Choi SUS (2006) Cooling performance of a micro-channel heat sink with nanofluids. *Appl Therm Eng* 26:2457–2463
17. Chein R, Chuang J (2006) Experimental micro channel heat sink performance studies using nanofluids. *Int J Ther Sci* 46:57–67
18. Wang Y, Ding GF (2008) Numerical analysis of heat transfer in a manifold microchannel heat sink with high efficient copper heat spreader. *Microsyst Technol* 14:389–395
19. Ho CJ, Wei LC, Li ZW (2010) An experimental investigation of forced convective cooling performance of a microchannel heat sink with Al₂O₃/water nanofluid. *Appl Therm Eng* 30:96–103
20. Namburu PK, Das DK, Tanguturi KM, Vajjha RS (2009) Numerical study of turbulent flow and heat transfer characteristics of nanofluids considering variable properties. *Int J Ther Sci* 48:290–302
21. Kandlikar SG, Garimella S, Li D, Colin S, King MR (2006) Heat transfer and fluid flow in minichannels and microchannels. Elsevier, Amsterdam. ISBN: 0-0804-4527-6
22. Das SK, Choi SUS, Yu W, Pradeep T (2009) Nanofluids Science and Technology. Wiley, New York. ISBN: 978-0-470-07473-2
23. Masuda H, Ebata A, Teramae K, Hishinuma N (1993) Alteration of thermal conductivity and viscosity of liquid by dispersing ultra-fine particles (dispersion of r-Al₂O₃, SiO₂, and TiO₂ ultra-fine particles). *Netsu Bussei (Japan)* 4:227–233
24. Li CH, Peterson GP (2009) Experimental investigation of temperature and volume fraction variations on the effective thermal conductivity of nano particle suspensions (nanofluids). *J Appl Phys* 99:084314-084314-8
25. Jang SP, Stephen SUS (2007) Effects of various parameters on nanofluid thermal conductivity. *J Heat Transf* 129:617–623
26. Dix J, Jokar A, Martinsen R (2008) Enhanced micro channel cooling for high power semiconductor diode lasers. SPIE LASE 6876-5, SPIE photonics west, San Jose, California